

A primitive placoderm sheds light on the origin of the jawed vertebrate face

Vincent Dupret¹, Sophie Sanchez^{1,2}, Daniel Goujet³, Paul Tafforeau² & Per E. Ahlberg¹

Extant vertebrates form two clades, the jawless Cyclostomata (lampreys and hagfishes) and the jawed Gnathostomata (all other vertebrates), with contrasting facial architectures^{1,2}. These arise during development from just a few key differences in the growth patterns of the cranial primordia: notably, the nasal sacs and hypophysis originate from a single placode in cyclostomes but from separate placodes in gnathostomes, and infraoptic ectomesenchyme migrates forward either side of the single placode in cyclostomes but between the placodes in gnathostomes^{3–8}. Fossil stem gnathostomes preserve cranial anatomies rich in landmarks that provide proxies for developmental processes and allow the transition from jawless to jawed vertebrates to be broken down into evolutionary steps^{7,9–12}. Here we use propagation phase contrast synchrotron microtomography to image the cranial anatomy of the primitive placoderm (jawed stem gnathostome) *Romundina*¹³, and show that it combines jawed vertebrate architecture with cranial and cerebral proportions resembling those of cyclostomes and the galeaspid (jawless stem gnathostome) *Shuyu*¹¹. This combination seems to be primitive for jawed vertebrates, and suggests a decoupling between ectomesenchymal growth trajectory, ectomesenchymal proliferation, and cerebral shape change during the origin of gnathostomes.

One of the most distinctive features of cyclostome facial architecture is the median nasohypophyseal duct, which forms when the posthypophyseal processes grow forward on either side of the nasohypophyseal placode to create the hood (lamprey) or oronasal membrane plus tentacles (hagfish)^{2,4–7}. In gnathostomes, by contrast, these processes converge in the midline between the hypophyseal and nasal placodes to create the trabeculae, while the maxillary process of the mandibular arch grows forward laterally to form the upper jaw^{1,4–7,14}. Cyclostomes have very short forebrains and nasal sacs that lie well posterior to the upper lip of the mouth, whereas gnathostomes have longer forebrains and nasal sacs located above the jaw margin^{4–7}. The cyclostome hypophysis projects ventrally into the nasohypophyseal duct, whereas the gnathostome hypophysis projects posteroventrally towards the palate; the distance between hypophysis and nasal sacs is thus much greater in gnathostomes than cyclostomes.

Comparative analysis of extant cyclostomes and gnathostomes alone does not allow us to polarize this transformation or break it down into steps. However, the lower part of the gnathostome stem group comprises fossil jawless vertebrates with nasohypophyseal ducts¹⁵, showing that the cyclostome pattern precedes the gnathostome pattern and indicating that fossils can potentially illuminate the transformation itself (Fig. 1 and Extended Data Figs 1 and 2). The 430-million-year-old galeaspid (jawless stem gnathostome) *Shuyu* seems to show an early transitional condition: nasal sacs and hypophysis are separated by a small trabecular process, but open into a common nasohypophyseal duct¹¹. This suggests that the posthypophyseal processes of *Shuyu* followed a lateral growth path as in cyclostomes, but that nasal and hypophyseal placodes were separate, and that a small component of the premandibular ectomesenchyme grew into the midline above the hypophyseal placode to form the trabecular process (Supplementary Information).

Placoderms (extinct armoured jawed fishes) form the paraphyletic upper part of the gnathostome stem group^{9,10,12}. They may thus include the most primitive examples of jawed vertebrate morphology. *Romundina stellina* Örvig, 1975 (ref. 13) (Fig. 2 and Extended Data Figs 3 and 4), from the earliest Devonian period (410–419 million years ago) of Canada, is one of a small number of placoderms that differ from all other jawed vertebrates by having nasal capsules positioned between the eyes, well behind the upper lip. These ‘posterior-nosed’ forms, which also include *Brindabellaspis* and antiarchs, are consistently recovered among the phylogenetically deepest placoderms^{9,10,12,15,16} (Fig. 1, Supplementary Information and Extended Data Figs 1 and 2). The position of the capsules suggests that they had short forebrains, but their endocranial anatomy has remained largely unknown^{15,17–19}. The only properly documented cranial cavity of a posterior-nosed form is that of *Brindabellaspis*, reconstructed from two acid-prepared braincases¹⁸. *Brindabellaspis* has some puzzling features, such as nasal sacs located within the orbits¹⁸, which make it difficult to assess whether its endocranial anatomy is representative for posterior-nose placoderms in general.

Here we present the braincase of *Romundina*, reconstructed from a propagation phase contrast synchrotron microtomography (PPC-SRμCT) scan of specimen MNHN CPW1 (Fig. 2a, b and Supplementary Video 1). The specimen is complete apart from an oblique ventral breakage and the absence of the rostronasal capsule. This capsule, comprising the nasal capsules and their dermal bone cover, was separated from the braincase by an encircling optic fissure (Fig. 2a, b); it is known

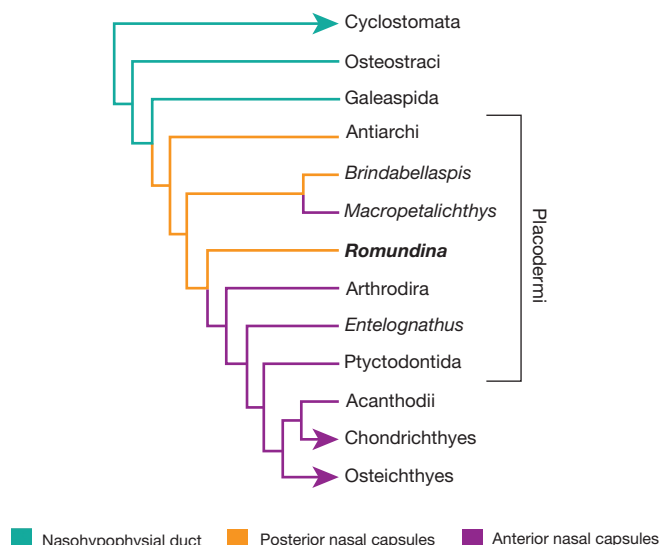


Figure 1 | Phylogenetic position of *Romundina*. Simplified vertebrate phylogeny, based on the character matrix reported previously¹² with the addition of *Romundina*, showing the distribution of different nasal architectures. Arrowheads indicate extant groups. For full analysis see Supplementary Information.

¹Uppsala University, Department of Organismal Biology, Subdepartment of Evolution and Development, Norbyvägen 18A, SE-752 36, Uppsala, Sweden. ²European Synchrotron Radiation Facility, 6 rue Jules Horowitz, 38043 Grenoble Cedex, France. ³Muséum national d'Histoire naturelle, Département Histoire de la Terre, Paléontologie, 8 rue Buffon, 75005 Paris, France.

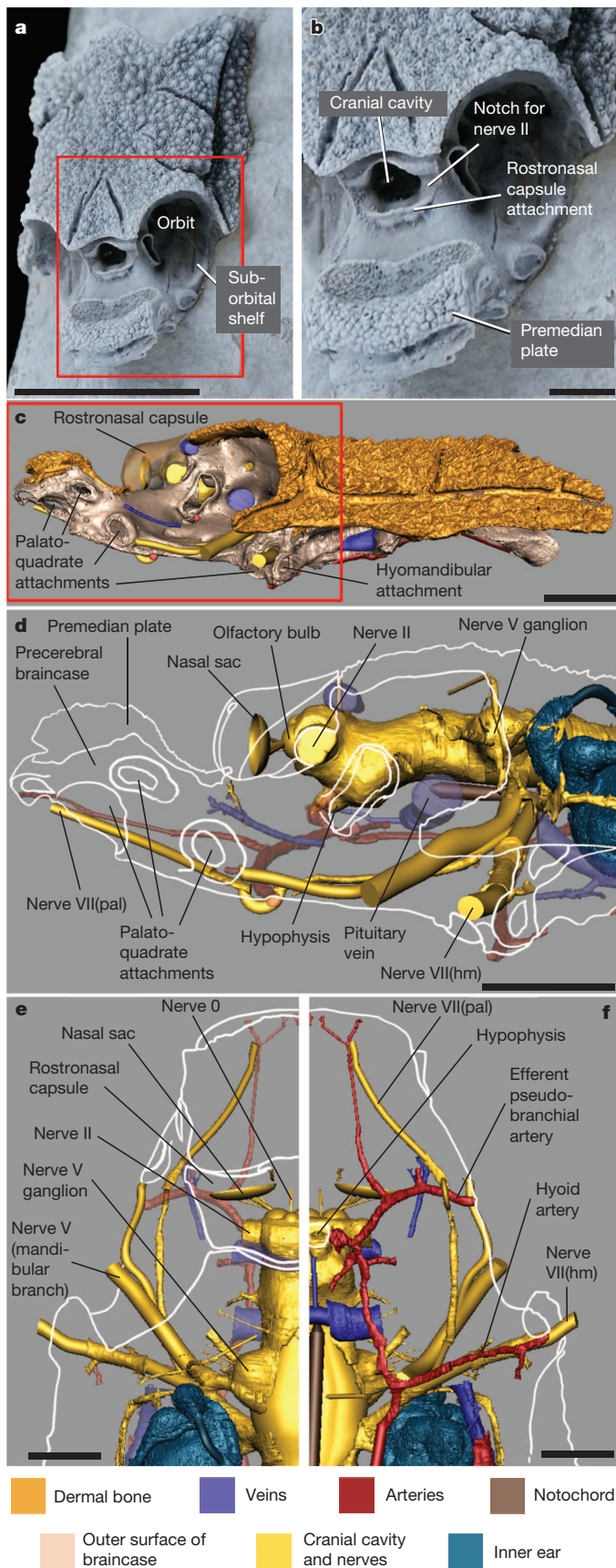


Figure 2 | Endocranial anatomy of *Romundina*. **a**, Photograph of specimen MNHN CPW1 in left anterodorsolateral view. The red box indicates the area enlarged in **b**. **b**, Orbital region and snout in close-up view. **c**, Braincase and skull roof in left lateral view, modelled from PPC-SRμCT scan. Red box indicates region shown in **d–f**. **d–f**, Cranial cavity and associated structures in lateral (**d**), dorsal (**e**) and ventral (**f**) views. Outline of braincase shown in white. Rostronasal capsule, nasal sacs and olfactory bulbs are reconstructed from previously reported data¹³ (see also Supplementary Information). **e** and **f** both extend slightly across the midline so that midline structures such as nerve 0 and the hypophyseal fossa are shown complete. Scale bars: **a**, 10 mm; **b–d**, 2 mm; **e, f**, 1 mm. All images are original.

braincase is broadly similar to those of other early placoderms^{15,17,21–23} and will be the subject of a subsequent publication. We focus here on the anterior region, from the canal for the hyomandibular branch of the facial nerve (VII(hm)) to the tip of the snout (Fig. 2d–f and Extended Data Fig. 3d–f), which differs radically from the corresponding region of an extant gnathostome.

The telencephalic portion of the cranial cavity is extremely short (Figs 2c–e, 3). It is bounded anteriorly by the lamina cribrosa of the rostronasal capsule (Extended Data Fig. 4 and ref. 13), which carries on its posterior face a central pair of foramina for the terminal nerve (nerve 0) and two lateral concavities for the olfactory bulbs. Posterior to the optic foramen (nerve II), which straddles the optic fissure, the diencephalic portion of the cranial cavity passes down to the anteroventrally directed hypophyseal recess. Large recesses for the nerve V ganglia mark the level of the pons. Nasal–hypophyseal distance is much smaller than in an extant gnathostome (Fig. 3). Similar proportions characterize the cranial cavities of the posterior-nosed placoderms *Brindabellaspis*¹⁸ and *Jagorina*²³, the galeaspid *Shuyu*¹¹, and the brains of extant cyclostomes¹⁵ (Supplementary Information). We conclude that cerebral proportions remained substantially unchanged through the transition from jawless to jawed cranial architecture, and that the characteristic elongate telencephalon and posteroventrally oriented hypophysis of extant gnathostomes evolved later (Fig. 3).

The braincase of *Romundina* includes a large precerebral region and broad suborbital shelves that terminate caudally at the canal for the hyomandibular branch of the facial nerve (nerve VII(hm)) (Fig. 2 and Extended Data Fig. 3). The suborbital shelves carry a series of articulations for the palatoquadrate (known from detached examples¹³) from the anterior end of the precerebral region to immediately in front of the VII(hm) nerve foramen. The spatial relationship of this region to the palatoquadrate and rostronasal capsule, and the fissure separating it from the latter, indicate that the precerebral braincase and suborbital shelves are formed by the trabeculae. In extant gnathostomes, the posterior part of the trabeculae consists of infraoptic ectomesenchyme, whereas the anterior part seems to contain varying components of supra- and infraoptic ectomesenchyme, depending on taxon^{24,25}; the nasal capsules are always composed of supraoptic ectomesenchyme. In *Romundina*, the sharp anterior demarcation and bounding fissure of the rostronasal capsule suggest that it formed the anteriormost part of the supraoptic ectomesenchyme and that the whole trabecular region was composed of infraoptic material (Supplementary Information and Figs 3 and 4).

The braincase of *Brindabellaspis* resembles that of *Romundina* in having a long precerebral region¹⁸. The partly preserved braincase of the antiarch *Minicrania* and attachment scars on the dermal skull bones of other antiarchs indicate a similar configuration^{19,26}. The rostronasal capsule was small and fissure bounded in antiarchs (as indicated by the dermal component), whereas in *Brindabellaspis* the capsule was fused to the braincase and the nasal sacs lay in the anterior corners of the orbits^{17,18}. We conclude that the anatomical interpretation and inferred ectomesenchymal map of *Romundina* are applicable to posterior-nosed placoderms in general.

Although *Romundina* is an unambiguous jawed vertebrate, the proportions of its brain closely resemble those of jawless vertebrates. Furthermore, its facial morphology suggests that the region formed from infraoptic ectomesenchyme was proportionately much larger than in an extant

from other specimens of *Romundina*^{13,20} (Extended Data Fig. 4), allowing us to reconstruct its position and internal spaces (Figs 2c–f and 3, Extended Data Fig. 3c–f and Supplementary Video 2). The posterior part of the

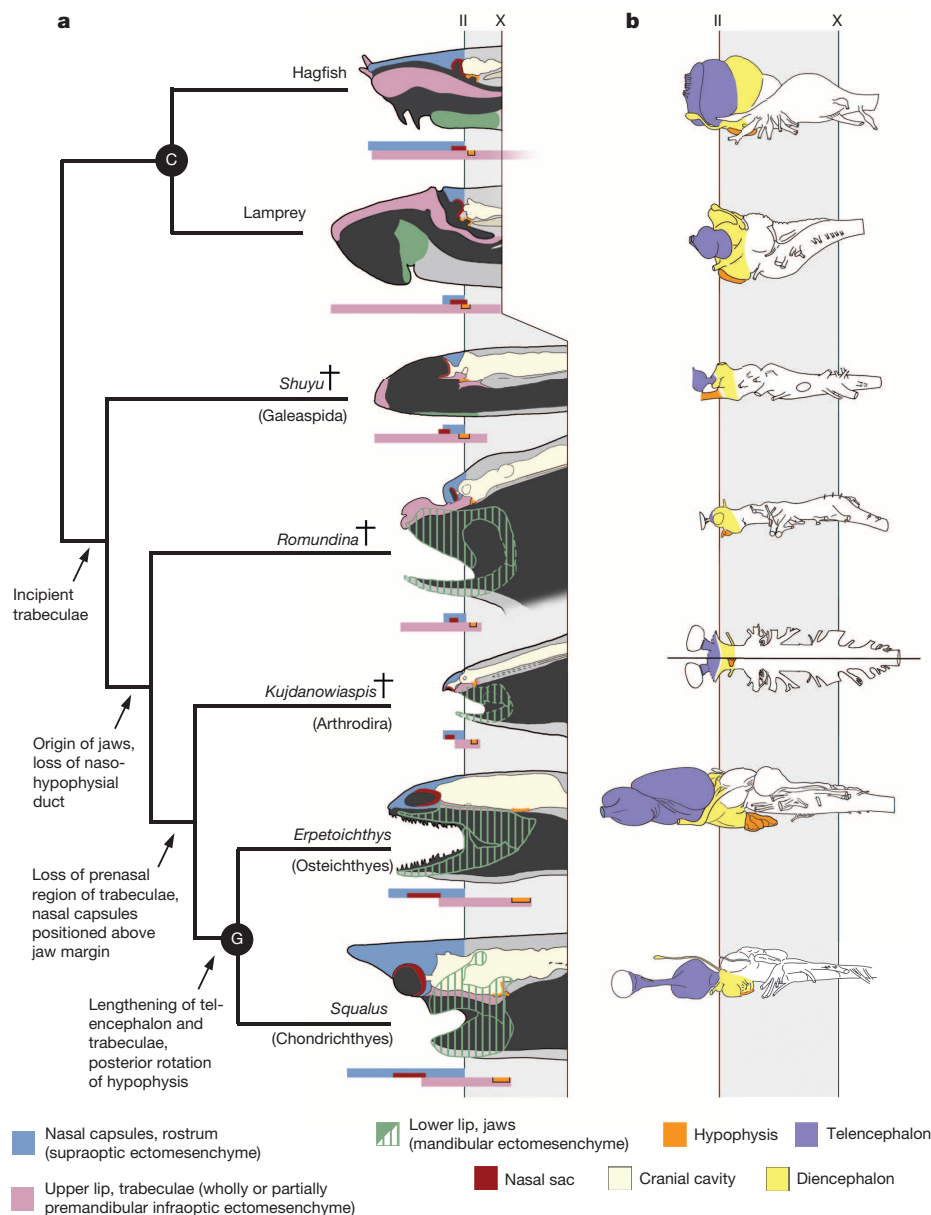


Figure 3 | Transformation of the vertebrate face and brain. **a**, Phylogeny of representative vertebrates, with diagrammatic sagittal sections of their heads. Heads are aligned on the exits of the optic nerve (II) and vagus nerve (X); cyclostomes are shown at a smaller scale because of their short brains and large precerebral regions. Bar diagram beneath each head shows the longitudinal position and extent of cranial components. Posterior boundary of supraoptic ectomesenchyme is positioned arbitrarily at the level of nerve II. Hagfish and lamprey are modified from ref. 7, Shuyu is based on data from ref. 11, with permission, all other images are original. C, cyclostome crown group node; G, gnathostome crown group node. Arrows indicate important evolutionary steps. **b**, Brains/cranial cavities of the same taxa, aligned on the optic nerve (II) and vagus nerve (X), all in lateral view except *Kujdanowiaspis*, which is shown in composite dorsal (top)/ventral (bottom) view because no lateral view is available. Diagrams of brains of hagfish, lamprey, *Erpetoichthys* are modified with permission from ref. 29; brain of *Squalus* is modified with permission from ref. 30; cranial cavity of Shuyu is modified with permission from ref. 11; cranial cavity of *Kujdanowiaspis* is modified from ref. 23.

gnathostome and projected anteriorly beyond the supraoptically derived rostronasal capsule (Figs 3 and 4). This resembles the condition in extant cyclostomes, where infraoptic material forms the bulk of the upper lip or oronasal membrane (Fig. 3). The phylogenetic position of *Romundina* and the similar morphology of other posterior-nosed placoderms suggest that these characteristics are primitive for jawed stem gnathostomes. Immediately crownward to *Romundina*, our phylogenetic analysis recovers the clade Arthrodira (Figs 1 and 3, Supplementary Information and Extended Data Figs 1 and 2). Primitive arthrodirans such as *Kujdanowiaspis*^{21,23} and *Dicksonosteus*²² have terminal rostronasal capsules, but their forebrains are still very short. Comparison with *Romundina* (Fig. 3) indicates that this configuration was produced by shortening the trabecular region anteriorly. In the gnathostome crown group the telencephalon, trabecular region and supraoptic ectomesenchymal territory have all been lengthened substantially, but their relative positions and proportions remain similar to those of arthrodirans (Fig. 3).

The transformation from cyclostome to gnathostome facial architecture has been described as a heterotopic phenomenon, involving changes in ectomesenchymal growth trajectories and ectoderm–ectomesenchyme interactions⁶. The data from stem gnathostomes support this interpretation but add evidence for the intermediate steps of the transformation and the decoupling of different processes (Fig. 3). Separate but closely

spaced nasal and hypophyseal placodes, associated with a short telencephalon, were established before the origin of jaws and retained an unchanged geometry across the transition from agnathans to jawed vertebrates. This shows that the heterotopic shift in ectomesenchymal growth trajectory, which replaced the nasohypophyseal duct with a solid trabecular region, was not driven by a lengthening of the telencephalon, leading to wider separation of the nasal and hypophyseal placodes. On the contrary, we suggest that the creation of a trabecular region contributed to making this lengthening possible. By forming a horizontal shelf between the nasal sacs and hypophysis, the trabeculae also became a skeletal floor for the telencephalic part of the cranial cavity, which could support and protect a long telencephalon. In cyclostomes the telencephalon has no ventral support⁷. Consonant with this hypothesis, telencephalic lengthening occurred independently at least twice among placoderms (in *Macropetalichthys* and pholidosteoid arthrodirans²³) as well as in crown gnathostomes. Even within the crown group, some early members such as the sarcopterygian *Tungsenia*²⁷ retain a relatively short telencephalon, although the nasal–hypophyseal distance is greater than in *Romundina* or primitive arthrodirans.

When the trabecular region first evolved, its dimensions were similar to an agnathan upper lip (Figs 3 and 4), suggesting that the change of growth trajectory for the premandibular ectomesenchyme was not

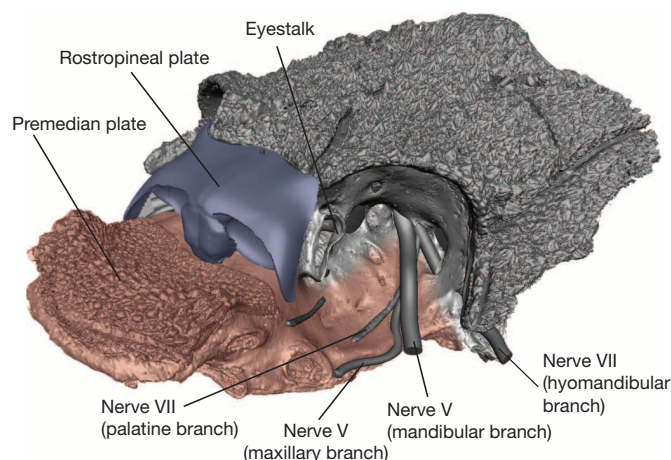


Figure 4 | Inferred neural crest composition of *Romundina*. PPC-SRμCT model of *Romundina* specimen MNHN CPW1 in left anterodorsolateral view, with reconstructed rostronasal capsule, showing inferred extent of premandibular infraoptic ectomesenchyme (pink) and supraoptic ectomesenchyme (blue).

initially associated with a reduction in cell proliferation to produce a smaller structure; relative size reduction of the trabeculae, which produced the spatial configuration characteristic of extant gnathostomes, came later. This implies that trajectories and proliferation patterns must have been regulated separately during the morphological transformation from jawless to jawed facial architecture. We predict that separate regulatory networks for these attributes are also present in extant vertebrates.

METHODS SUMMARY

Specimens of *Romundina stellina* were partly freed from the surrounding limestone matrix by dilute formic acid. One specimen was imaged with PPC-SRμCT at beamline ID19 of the European Synchrotron Radiation Facility (see Supplementary Information and ref. 28 for technical specifications). Mimics v.12.3 and v.13.1 (Materialise) were used for three-dimensional modelling. Pictures and animations were rendered in Maya 2012 (Autodesk).

Online Content Any additional Methods, Extended Data display items and Source Data are available in the online version of the paper; references unique to these sections appear only in the online paper.

Received 30 July; accepted 30 December 2013.

Published online 12 February 2014.

- Kuratani, S. & Horigome, N. Development of peripheral nerves in a cat shark, *Scyliorhinus torazame*, with special reference to rombomeres, cephalic mesoderm, and distribution patterns of crest cells. *Zoolog. Sci.* **17**, 893–909 (2000).
- Kuratani, S., Horigome, N. & Hirano, S. Developmental morphology of the head mesoderm and re-evaluation of segmental theories of the vertebrate head: evidence from embryos of an agnathan vertebrate, *Lampetra japonica*. *Dev. Biol.* **210**, 381–400 (1999).
- Kuratani, S. Evolution of the vertebrate jaw: comparative embryology and molecular developmental biology reveal the factors behind evolutionary novelty. *J. Anat.* **205**, 335–347 (2004).
- Kuratani, S. Developmental studies of the lamprey and hierarchical evolutionary steps towards the acquisition of the jaw. *J. Anat.* **207**, 489–499 (2005).
- Kuratani, S. Evolution of the vertebrate jaw from developmental perspectives. *Evol. Dev.* **14**, 76–92 (2012).
- Kuratani, S., Nobusada, Y., Horigome, N. & Shigetani, Y. Embryology of the lamprey and evolution of the vertebrate jaw: insights from molecular and developmental perspectives. *Phil. Trans. R. Soc. Lond. B* **356**, 1615–1632 (2001).

- Oisi, Y., Ota, K. G., Kuraku, S., Fujimoto, S. & Kuratani, S. Craniofacial development of hagfishes and the evolution of vertebrates. *Nature* **493**, 175–180 (2013).
- Ota, K. G. & Kuratani, S. Cyclostome embryology and early evolutionary history of vertebrates. *Integr. Comp. Biol.* **47**, 329–337 (2007).
- Brazeau, M. D. The braincase and jaws of a Devonian ‘acanthodian’ and modern gnathostome origins. *Nature* **457**, 305–308 (2009).
- Davis, S. P., Finarelli, J. A. & Coates, M. I. Acanthodes and shark-like conditions in the last common ancestor of modern gnathostomes. *Nature* **486**, 247–250 (2012).
- Gai, Z., Donoghue, M. J., Zhu, M., Janvier, P. & Stampanoni, M. Fossil jawless fish from China foreshadows early jawed vertebrate anatomy. *Nature* **476**, 324–327 (2011).
- Zhu, M. et al. A Silurian placoderm with osteichthyan-like marginal jaw bones. *Nature* (2013).
- Ørving, T. in *Problèmes Actuels de Paléontologie: Evolution des Vertébrés* (ed. Lehman, J. P.) 41–72 (Colloques Internationaux Centre National de la Recherche Scientifique, 1975).
- Couly, G. F., Coltey, P. M. & Le Douarin, N. M. The triple origin of skull in higher vertebrates: a study in quail-chick chimeras. *Development* **117**, 409–429 (1993).
- Janvier, P. *Early Vertebrates* Vol. 1 (Clarendon, 1996).
- Goujet, D. & Young, G. C. Interrelationships of placoderms revisited. *Geobios*. **28**, 89–95 (1995).
- Denison, R. H. *Placodermi* (Gustav Fischer, 1978).
- Young, G. C. A new Early Devonian placoderm from New South Wales, Australia, with a discussion of placoderm phylogeny. *Palaeontographica* **167**, 10–76 (1980).
- Young, G. C. Reconstruction of the jaws and braincase in the Devonian placoderm fish *Bothriolepis*. *Palaeontology* **27**, 635–661 (1984).
- Goujet, D. & Young, G. C. in *Recent Advances in the Origin and Early Radiation of Vertebrates* (eds Arratia, G., Wilson, M. V. H. & Cloutier, R.) 109–126 (Dr. Friedrich Pfeil, 2004).
- Dupret, V. Revision of the genus *Kujdanowiaspis* Stensiö, 1942 (Placodermi, Arthrodira, “Actinolepida”) from the Lower Devonian of Podolia (Ukraine). *Geodiversitas* **32**, 5–63 (2010).
- Goujet, D. *Les Poissons Placodermes du Spitzberg: Arthrodira Dolichothoraci de la Formation de Wood Bay (Devonien Inférieur)* (CNRS, 1984).
- Stensiö, E. in *Traité de Paléontologie* Vol. 4 (ed. Piveteau, J.) 71–693 (Masson, 1969).
- Osumi-Yamashita, N. et al. Cranial anomaly of homozygous *rSey* rat is associated with a defect in the migration pathway of midbrain crest cells. *Dev. Growth Differ.* **39**, 53–67 (1997).
- Wada, N., Nohno, T. & Kuratani, S. Dual origin of the prechordal cranium in the chicken embryo. *Dev. Biol.* **356**, 529–540 (2011).
- Zhu, M. & Janvier, P. A small antiarch, *Minicrania lirouyii* gen. et sp. nov. from the early Devonian of Qujing, Yunnan (China), with remarks on the antiarch phylogeny. *J. Vertebr. Paleontol.* **16**, 1–15 (1996).
- Lu, J. et al. The earliest known stem-tetrapod from the Lower Devonian of China. *Nature Commun.* **3**, 1160 (2012).
- Dupret, V., Sanchez, S., Goujet, D., Tafforeau, P. & Ahlberg, P. Bone vascularization and growth in placoderms (Vertebrata): the example of the premedian plate of *Romundina stellina* Ørving, 1975. *C. R. Palevol* **9**, 369–375 (2010).
- Collins, S. P. in *Fish Physiology* (eds McKenzie, D. J., Farrell, A. P. & Brauner, C. J.) 121–179 (Elsevier, 2007).
- De Iuliis, G. & Pulerà, D. *The Dissection of Vertebrates—A Laboratory Manual* (Academic, 2007).

Supplementary Information is available in the online version of the paper.

Acknowledgements We thank the European Synchrotron Radiation Facility for granting us beam time at ID19 (proposal EC-203). P.E.A., V.D. and S.S. acknowledge the support of European Research Council Advanced Investigator Grant 233111 and a Wallenberg Scholarship from the Knut and Alice Wallenberg Foundation, both awarded to P.E.A. We thank B. Ryll, M. Kundrat and H. Blom at Uppsala University for discussions. Specimen MNHN CPW 1 photographs were taken by P. Loubry (Centre National pour la Recherche Scientifique, Muséum national d'Histoire naturelle, Paris).

Author Contributions The project was conceived by V.D., P.E.A. and S.S. Specimens of *Romundina* were collected by D.G. Scanning and reconstruction of data sets were carried out by S.S. and P.T., with minor contributions to the scanning by V.D. and P.E.A. Three-dimensional modelling, rendering and animation were done by V.D., who also carried out phylogenetic analysis and anatomical interpretation with input from P.E.A. P.E.A. led the comparative developmental interpretation. P.E.A. and V.D. wrote the text. All authors critically reviewed the manuscript and approved the final draft.

Author Information Data are deposited online at <http://paleo.esrf.eu>. Reprints and permissions information is available at www.nature.com/reprints. The authors declare no competing financial interests. Readers are welcome to comment on the online version of the paper. Correspondence and requests for materials should be addressed to V.D. (vincent.dupret@ebc.uu.se) or P.E.A. (per.ahlberg@ebc.uu.se).

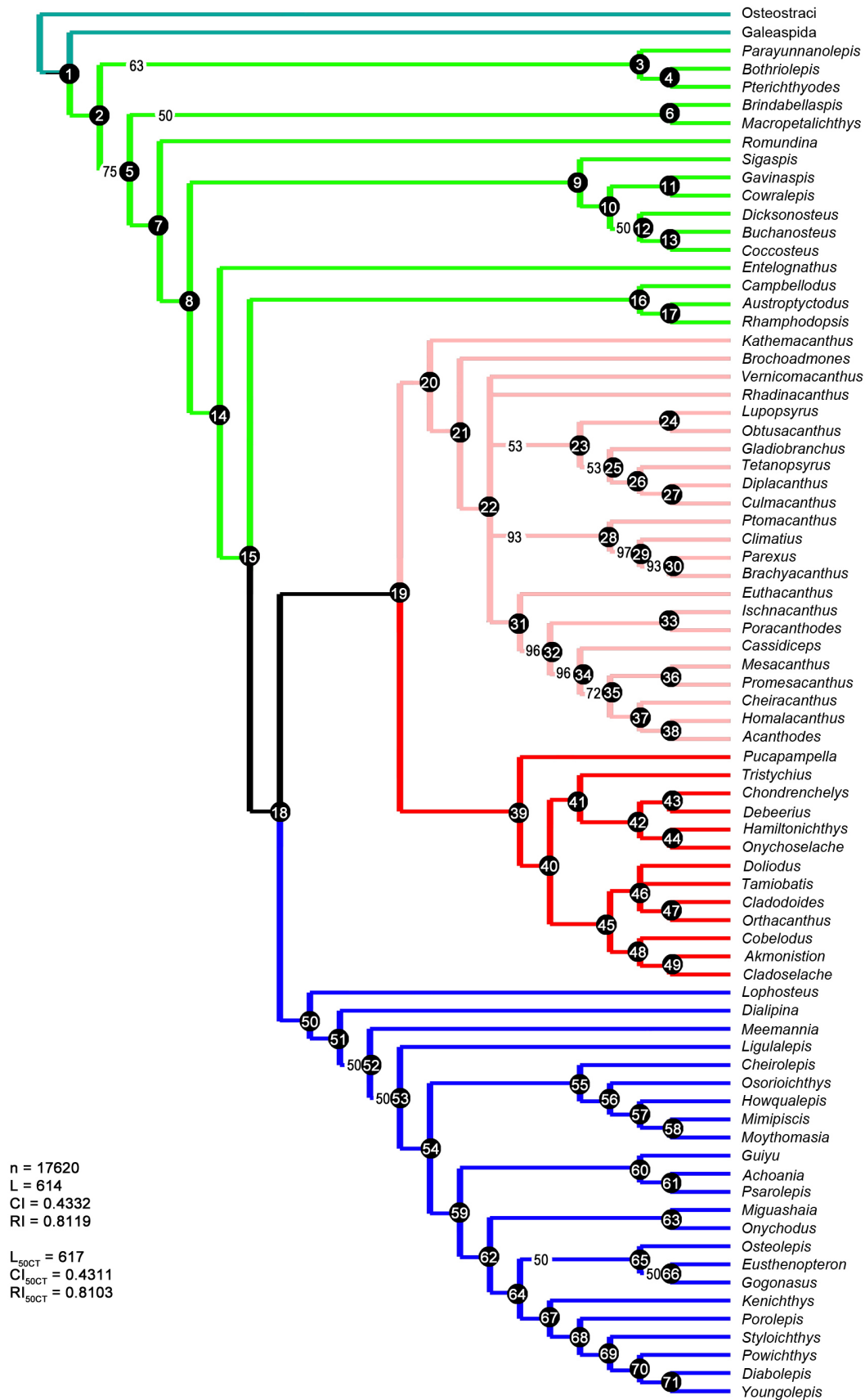
METHODS

Acquisition and reconstruction of the PPC-SR μ CT data set. The scan data set has an isotropic voxel size of 7.46 μm and was made using a monochromatic beam with an energy of 51 keV using a double Si111 crystal monochromator in Bragg reflection. The distance between sample and detector was 900 mm. A total of 1,999 projections over 360 degrees was taken with a FreLoN CCD camera, with 0.9 s of exposure time per projection. To image the complete specimen, four scans covering 7 mm vertically each were performed. The slices were reconstructed using a filtered back projection algorithm (PyHST software). The reconstructed slices were then converted into 16 bits .tif image stacks that were concatenated to obtain a single stack covering the whole sample. To reduce the data size for general anatomical observations, a second version of the reconstructed scan was calculated with a $2 \times 2 \times 2$ binning and an 8 bits conversion.

Anatomical reconstruction. In addition to structures (bone and space fills) that were modelled as preserved, the final three-dimensional model includes areas of

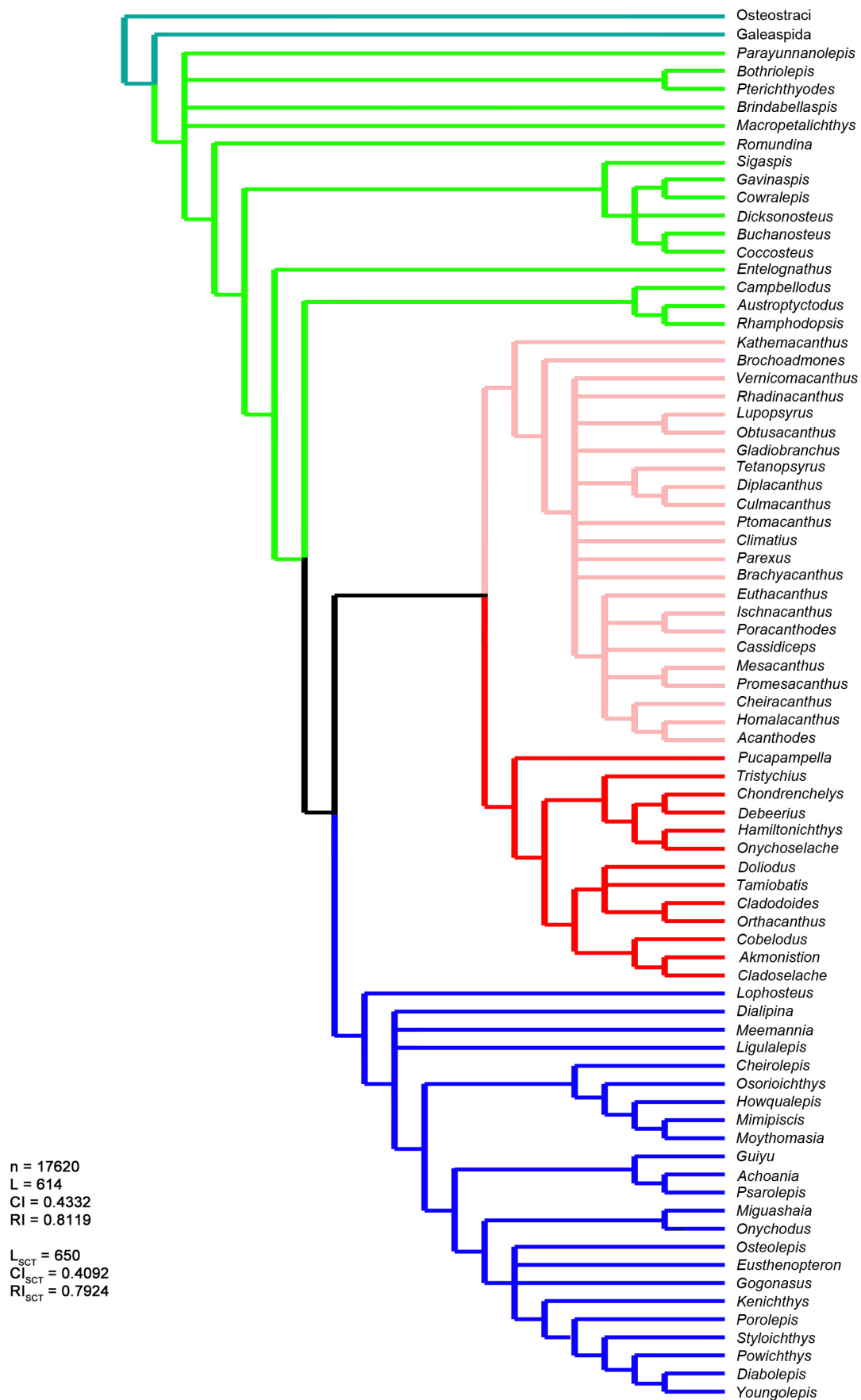
reconstruction produced by left/right mirroring of structures that are only preserved on one side, and some prosthetics. Mimics v.12.3 and v.13.1 (Materialise) were used for the three-dimensional modelling (segmentation, three-dimensional object rendering and STL polygon creation). Maya 2012 (Autodesk) was used for extra editing of the STLs (colour, texture, corrections) and kinematics, as well as for mirroring and the construction of prosthetics.

Mirroring, which was particularly useful as a remedy for information loss caused by the oblique break across the specimen, requires a certain amount of positional and morphological adjustment because the specimen is not perfectly bilaterally symmetrical. The prosthetics of the rostronasal capsule and other reconstructed structures (for example, the nasal sacs and the anterior face of the telencephalon) have all been given smooth, geometric surfaces to distinguish them from actual scanned anatomy. All are based on preserved correlates, such as cavities in the rostrorhinal capsule or nerve grooves on the subocular shelves of the braincase.

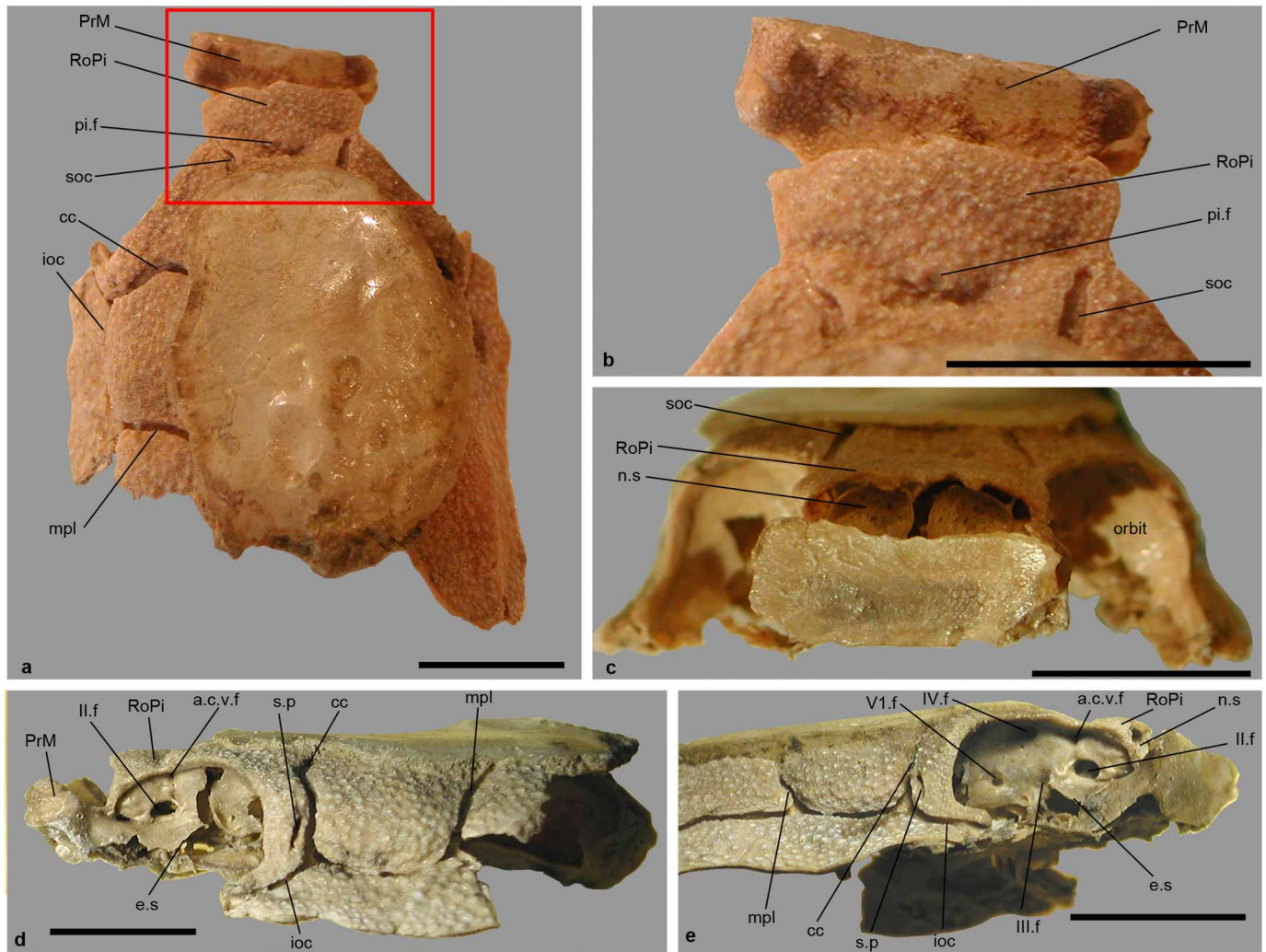


Extended Data Figure 1 | Majority rule (50%) consensus tree of the 17,620 most parsimonious trees from the phylogenetic analysis. Numbers at nodes (white on black filled circle) indicate nodes for character state changes described in Supplementary Information. Numbers on branches (black on

white) indicate the occurrence percentage of these branches in the 17,620 trees described in Supplementary Information. Jawless stem Gnathostomata ('ostracoderms') are in turquoise blue, Placodermi in green, Acanthodii in pink, Chondrichthyes in red, and Osteichthyes in blue.



Extended Data Figure 2 | Strict consensus tree of the 17,620 most parsimonious trees from the phylogenetic analysis.



Extended Data Figure 4 | *Romundina stellina* Orvig, 1975 (ref. 13)
(specimen MNHN CPW 13). **a–e**, Near complete skull roof with rostronasal caspule in articulation. **a, b**, Specimen in dorsal view (red box magnified in **b**). **c**, Specimen in anterior view. **d**, Specimen in left lateral view. **e**, Specimen in right lateral view. Il.f, optic nerve foramen; V1.f, profundus nerve foramen; IV.f, trochlear nerve foramen; III.f, oculomotor nerve foramen; a.c.v.f, anterior

cerebral vein foramen; cc, central sensory line groove; e.s, eyestalk; ioc, infraorbital sensory line groove; mpl, middle pitline groove; n.s, nasal sac; pi.f, pineal fontanelle; PrM, premedian plate; RoPi, rostrompineal plate; soc, supraorbital sensory line groove; s.p, sensory pit. Photographs of specimen MNHN CPW 13 were taken by D. Goujet.